applied sciences

MDPI

Article

Automation of a Hybrid Control for Electrohydraulic Servo-Actuators with Residual Dynamics

Lilia Sidhom [1,2], Ines Chihi [3,*] and Mohamed Smaoui [4]

1 Laboratory of Energy Applications and Renewable Energy Efficiency (LAPER), El Manar University, Tunis 1068, Tunisia; lilia.sidhom@enib.rnu.tn
2 Mechanical Department, Engineering School of Bizerte, University of Carthage, Carthage 1054, Tunisia
3 Department of Engineering, Campus Kirchberg, Faculté des Sciences, des Technologies et de Médecine, Université du Luxembourg, 1359 Luxembourg, Luxembourg
4 AMPERE Laboratory UMR 5005, INSA Lyon, 69621 Lyon, France; mohamed.smaoui@insa-lyon.fr
* Correspondence: ines.chihi@uni.lu

Abstract: In this paper, a hybrid position/force controller for electrohydraulic servo-actuators is designed in the presence of residual dynamics. The purpose is to apply a cycle of movement that is mostly used in industrial fatigue test applications, which consists in imposing a specified force on a flexible load after a movement to some position. This cycle can be repeated several times with different magnitudes and frequencies of force and position trajectories. Some damages could occur at switching times, especially in the presence of some residual dynamics. To avoid any damages at switching times, a force trajectory generator is designed. Then, our contribution defines a method to automatically generate the switching signal in order to commute between two controllers with any abrupt change of state. To show the effectiveness of the proposed approach, several simulation tests are carried out on the electrohydraulic system.

Keywords: hybrid control position/force; residual dynamics; trajectory generator; electrohydraulic system; simulation results

check for updates

Citation: Sidhom, L.; Chihi, I.; Smaoui, M. Automation of a Hybrid Control for Electrohydraulic Servo-Actuators with Residual Dynamics. *Appl. Sci.* **2022**, *12*, 2856. https://doi.org/10.3390/app12062856

Academic Editor: Alessandro Gasparetto

Received: 16 January 2022
Accepted: 8 March 2022
Published: 10 March 2022

1. Introduction

The compactness, high force-to-mass ratio and reliable performance of hydraulic actuators are factors that could potentially be exploited in a sophisticated manipulator design and many industrial applications. The dynamic behavior of electrohydraulic systems is highly nonlinear [1]. Therefore, the complexity of such systems and the important range of control laws are a real industrial problem where the target is to choose the best control strategy for a specific application. Depending on the sought specification, the displacement, the velocity, the force or the stiffness could then be considered as a variable control. In recent years, research efforts have been directed toward meeting these requirements. Most of these studies have been based on the linear control theory [2–5]. However, in such works, some important dynamic information may be lost when the hydraulic servo system is linearized around some operating point during the design. Therefore, it is important to choose a nonlinear control method that is reasonably suitable for hydraulic servo systems. A number of investigations have been conducted on feedback linearization techniques [6,7], adaptive control [8–10], backstepping control [11–15], sliding mode control [16–19] and controller design via quantitative feedback theory [20,21]. The objectives of the above-mentioned works are oriented to the control of either position or effort. Little applications that are aimed at both position and effort tracking problems also exist. A great deal of research arises from robotic problems where position control is required for stiffness and force control is designed for compliance [22–25]. Generally, in robotic applications, when the manipulator arm is sufficiently rigid, the considered hybrid control position/force is presented by a local control of the manipulator arm of each actuator articulation [22]. This gives some degree of decoupling between the position and effort controls. In Ref. [26], using the model-based control, different effort and position control schemes were developed. This suggested control loop was defined by a modified classical P + PID scheme, which has achieved good tracking performance. On the other hand, the effort and position control problem was treated separately, and the switching problem was then not considered. In Ref. [27], the authors presented the control of integrated electrohydraulic servo-drivers via conventional structures of PI and PD in order to separately control effort and position, respectively. The stability proof was not given. The parameters of these structures were calculated via indirect adaptive methods. These methods used identification tools and two control models with requirements for both effort and position tracking. Good performance was recorded for position control, but, for the effort controller, tracking remained efficient only for very low pulsation desired trajectories. Furthermore, the indirect adaptive schemas always have some issues with initial conditions. To overcome such issues and comparing the indirect adaptive method to the multiple PID controller approach, which is sensitive to its parameters, various solutions have been proposed in the literature [28]. In this last one, the authors proposed a multi-input multi-output (MIMO) controller based on fuzzy logic. The effort and position controls were independently tested and provided satisfactory results while consuming less energy. In Ref. [29], a hybrid position/force controller for joint robots based on a decoupling approach was presented. In fact, this approach used a smooth and invertible mapping linking the joint space to the task space in order to design the controllers separately. In Ref. [30], a literature review of the hydraulic control, specifically for manipulator robots, was detailed.

Other than the separate hybrid position/effort control approaches, control based on the switching signal approach is considered in this paper. The challenge here consists in controlling the position as well as the second derivative of the position of the same cylinder.

Some relevant research works can be cited in the literature. For example, in Ref. [31], the authors synthesized a hybrid position/force controller and applied it to an electropneumatic system. In this research work, the important purpose was to move a load near a rigid structure and apply a force against it without damages in the process. The control algorithm presented in this paper concerns a linear state feedback strategy for tracking both position and force. In this study, the switching position/effort controllers are carried out only according to the desired position. It should be noted that, despite the satisfaction tracking performance, a large peak of effort and position remains present during the switch occurrences. Recently, we have developed a hybrid position/force controller for a hydraulic actuator [32]. The idea here is defined by a global hybrid position/force control structure design based on a reduced state-space linear model. For such a design, the control parameters are determined separately as having the performances required in each configuration. In addition, autonomous switching is elaborated via a hysteresis relay where the switching is triggered by a hard stop. Despite the simplicity of the designed feedback controller, it is noteworthy to indicate the local character of such an algorithm, which leads to working on a limited domain of an operating range of the system. In addition, the control gain settings are determined via the standard pole placement for both position and force modes. Consequently, any change in the operating point requires a re-calculation of these gains. On the other hand, the stability proof remains locally limited to the operating points relating to the specific tests that are carried out. Although the tracking performance of the proposed controller is good, the force trajectory presents some overshoot at switching times. In Ref. [33], the authors circumvented the so-called stick-slip problem on the electropneumatic actuator with empirical switching controllers. To prove the stability, the closed-loop system was described in a piecewise-affine form to find a Lyapunov function for it.

There are several tools in the literature for analyzing the stability of a switched system. A survey of basic problems on the stability and design of switched systems has been proposed in Refs. [34,35]. In Refs. [36,37], the authors introduced the concept of hybrid systems and some challenges associated with the stability of such systems. In Ref. [38], the stability condition with multiple Lyapunov functions for switched systems was considered.

The stability proof using these methods is conditioned by the resident time of every subsystem that must be supposed relatively small. Otherwise, the stability can only be checked.

It is well known that the choice of the switching signal is important regardless of the switching type. For the time-dependent switching controller, a close relationship exists between the switching times and the design of the desired trajectories imposed on the process. Usually, the switching occurrences are manually adjusted to commute between different subsystems, but, in real-time applications, some state problems may appear [28]. Such problems can be so dangerous as to harm some sensors on the test bench. Moreover, these problems become more serious in the presence of some residual dynamics. Supposing that these uncontrolled dynamics are stable, the problem amounts exactly to the convergence time of these dynamics. In most of the previous works, switching was defined by imposing either the instants of switching or conditions on the system states. Such a switching choice does not prevent the appearance of undesirable peaks during switching. Our work is different to previous works since it proposes a purely mathematical solution, which allows automatically updating the desired force trajectory by taking into account the time of convergence of the residual dynamics. In this paper, the problem of time-dependent switching hybrid controller position/force is considered for electrohydraulic servo-actuator systems with a flexible load. The presence of such a load makes it possible to have uncontrolled states on the dynamics of one subsystem. To avoid any damage at switching times, our proposed solution is to design a force trajectory generator that is based on the desired position trajectory, previous switching times and time convergence of residual dynamics where it is computed in real time. Thus, our contribution is to conceive a specified switching law to guarantee system commutation without any problems.

The outline of this paper is as follows. Section 2 presents the system dynamics, including an electro-hydraulic servo-actuator. The problem formulation and illustration is taken care of in Section 3. In Section 4, two different control algorithms are synthesized for tracking the trajectory of both the position and the effort using, respectively, the back-stepping technique and the Lyapunov approach. The stability of the overall system is also checked. In the next section, the proposed solution is explained. Section 5 is dedicated to the simulation results.

2. Electrohydraulic Servo-Actuator Model

The considered system is presented in Figure 1. It is a symmetric double-acting electro-hydraulic servo-drive that uses a double-rod cylinder with a stroke of 330 mm, which is controlled by a five two-way servo-valve. The characteristics of the hydraulic actuator are given in Table A1 (see Appendix A).

This system disposes of some interface block between the actuator and the servo-valve. The presence of this block, which is specifically designed for the test bench to implement two servo-valves, makes it possible for the system to have three operating modes. Indeed, the actuator chambers can be fed either by a 5/2 single servo-valve (mode 1) or by two servo-valves in parallel to increase the flow (mode 2). The servo-valves can also be used in a three-way mode to supply flow independently to each actuator chamber (mode 3). In this paper, a single mode is considered to control the actuator by one 5/2 servo-valve (mode 1).

Although the interface block has an advantage over the system, its presence in this last one conduces to some pressure drop between the servo-valve and the cylinder chambers.

This pressure drop depends on the geometrical characteristics of different pipes that constitute the block, the velocity of the fluid and the input signal. For this reason, the output flow (Q_{11}, Q_{12}) of the servo-valve is different from the input flow ((Q_1, Q_2)) of the actuator (see Figure 1). In this work, this intermediate block is simply approximated to a resistive component, which is described by some constant that is determined experimentally.

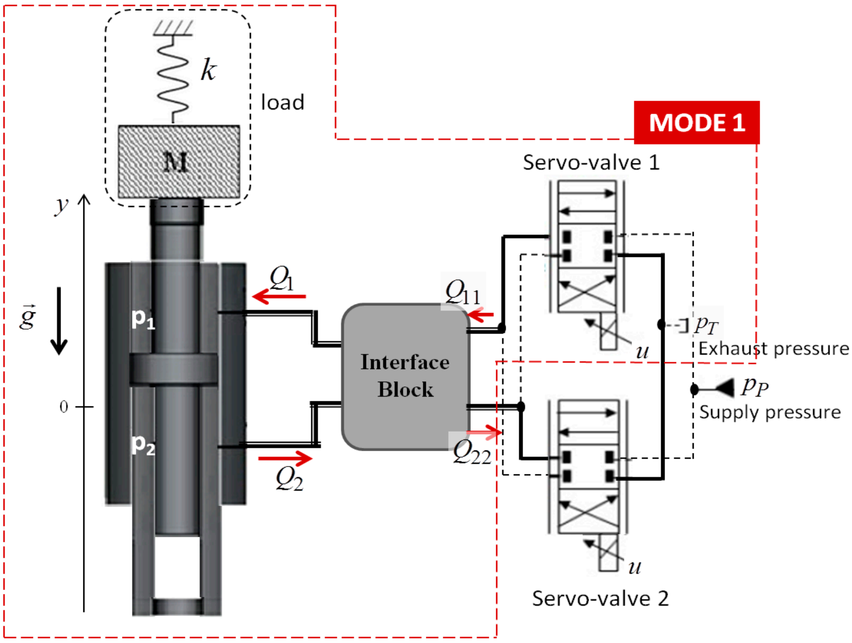

Figure 1. The schematic diagram of the hydraulic system.

According to Newton's second law, the dynamics of the inertia load can be described by:

$$Ma = S\Delta p - Mg - bv - ky + h \tag{1}$$

where y [m], v [m·s^{-1}] and a [m·s^{-2}] are, respectively, the displacement, the velocity and the acceleration of the load, M is the mass of the moving part, $\Delta p = p_1 - p_2$ is the pressure drop across the load piston, S is the effective area of the actuator chambers, k [N/m] is the stiffness load and b [N/m·s^{-1}] represents the coefficient of the viscous friction force. Dry friction forces h depend explicitly on the velocity and can be represented by the function $h(v(t))$. The empirical model of the friction effort, which is described by a smooth function such as *thanh*(.), is given in Ref. [33]. In fact, according to the Tustin friction model, $h(v(t))$ can be defined by such nonlinear function, [36]: $h(v(t)) = [F_{sdy} + (F_{sdy} - F_{Co})e^{-C|v(t)|}thanh\left(\frac{v(t)}{v_{i0}}\right)$. Where F_{sdy} and F_{Co} are the dynamic dry friction and the Coulomb friction, respectively. C and v_{i0} are the coefficient of the Stribeck effect and the velocity scaling constant, respectively.

In our case, the dry friction is neglected.

In a variable volume chamber, the obtained equation flows rely on some assumptions, viz.: (A1) both the temperature and pressure of the oil are homogeneous in each chamber, (A2) the oil density variation is small compared to its average density, (A3) the temperature variation is small compared to the average temperature, which is equal to the oil supply temperature. According to these assumptions, and neglecting leakage flows, the governing nonlinear equations that describe the fluid flow distribution in the servo-valve can be written as follows [1]:

$$\begin{cases} Q_1 = \frac{V_1(y)}{\beta}\frac{dp_1}{dt} + \frac{dV_1}{dt}, \\ Q_2 = \frac{V_2(y)}{\beta}\frac{dp_2}{dt} + \frac{dV_2}{dt} \end{cases} \tag{2}$$

β is the effective Bulk modulus. V_1 and V_2 are the total volumes of the cylinder defined, respectively, by:

$$\begin{cases} V_1(y) = V_0 + Sy, \\ V_2(y) = V_0 - Sy, \end{cases} \tag{3}$$

where:

$$V_0 = V_D + S\frac{l}{2} \tag{4}$$

is the piping volume of each chamber for the zero position and V_D is a dead volume present on each extremity of the cylinder. Considering that the interface block is symmetric, then its piping volume is also taken account of by V_0.

In our case, the servo-valve has a large frequency of about 1 kHz. Consequently, it can be neglected in front of the slow dynamics of the actuator whose open-loop average frequency in the central position is about 250 Hz. This is why the spool valve displacement x_t is assumed to be directly related to the control voltage u, with a proportional relationship defined by the gain K_{sv}, viz.: $x_t = K_{sv}\ u$. This kind of assumption can be used in control for some operating modes [1]. Then, the flow laws can be given in affine form:

$$\begin{cases} Q_1 = r\psi_1(sign(u), p_1, p_P, p_T) \\ Q_2 = -r\psi_2(sign(u), p_2, p_P, p_T) \end{cases} \tag{5}$$

where:

$$\begin{cases} \psi_1(.) = \alpha\left[h(u)\sqrt{|p_P - p_1|}sign(p_P - p_1) + h(-u)\sqrt{|p_1 - p_T|}sign(p_1 - p_T)\right] \\ \psi_2(.) = \alpha\left[h(u)\sqrt{|p_T - p_2|}sign(p_T - p_2) + h(-u)\sqrt{|p_P - p_2|}sign(p_P - p_2)\right] \end{cases} \tag{6}$$

With: $h(u) = \frac{1+sign(u)}{2}$ and the function $sign(u)$ defined by:

$$sign(u) = \begin{cases} 1 & \forall u \geq 0, \\ -1 & \forall u < 0 \end{cases} \tag{7}$$

The servo-valve is supposed to be a symmetric one, which justifies the presence of the same variable gain in the two flow laws. The coefficient of the flow gain r is defined by the expression $r = \omega\phi$, is the spool valve area gradient, and ϕ is the pressure drop caused by the interface block.

Let us define the variable $\alpha = C_{d\infty}K_{sv}\sqrt{2/\rho}$, which is assumed to be a constant parameter, where ρ is the fluid density and $C_{d\infty}$ is the flow coefficient constant of each restriction. Note that the defined parameters α, r are supposed to be constant.

We note the physical domain of the system by:

$$D_\varphi = \left\{(y, v, \Delta P) \in IR^3 / |y| \leq \frac{l}{2}, p_1, p_2 \in \Omega_p \equiv]p_T, p_P[\right\} \tag{8}$$

Considering D_φ, the terms $sign(p_P - p_j)$ and $sign(p_j - p_T), \quad j = \{1, 2\}$ introduced in the expression of ψ_1 and ψ_2 (Equation (6)) can be deleted as well as the absolute values.

Let us define the state variables $X = [y, v, \Delta P]'$, and the system can then be expressed in the form below:

$$\dot{X} = f(X) + g(X)u, \tag{9}$$

With $X, f(X), g(X) \in \mathbb{R}^3$, $u \in \mathbb{R}$, where $f(X), g(X)$ are locally Lipschitz vector fields, defined by:

$$f(X) = \begin{pmatrix} v \\ \frac{1}{M}[S\Delta P - Mg - bv - ky] \\ -\beta S\left[\frac{1}{V_1(y)} + \frac{1}{V_2(y)}\right] \end{pmatrix}$$

$$g(X) = \begin{pmatrix} 0 \\ 0 \\ \beta\left[\frac{r\psi_1(.)}{V_1(y)} + \frac{r\psi_2(.)}{V_2(y)}\right] \end{pmatrix}$$

And b is the coefficient of the viscous friction force, and k is the stiffness load.

3. Problem Statement and Illustration

Our research work is addressed to control the electrohydraulic system in touch with a flexible load described above by switching the input signal between the position and the effort.

3.1. Problem Statement

The main idea provides a tracking performance while maintaining the stability of the overall system with any problem at the switching times.

For this purpose, let us define the model system as follows:

$$\begin{cases} \dot{X} = f(X) + g(X)u_p, & (S_1) \\ \dot{X} = f(X) + g(X)u_F, & (S_2) \end{cases} \tag{10}$$

For the control position target, the subsystem (S_1) is then defined as in (10), with u_p its input signal. When this target is changed to the effort control, the system will be described by the subsystem (S_2), where u_F is the new input signal to track some force-desired trajectory.

Note that, owing to the system order, which is equal to three compared to the relative degree for (S_2), which is equal to one, this subsystem presents second-order residual dynamics. Then, the problem here arises when switching takes place from the force controller to the position controller.

Consequently, this hybrid controller needs to be implemented for switching to occur between the position and force controllers with some operating phases, with an appropriate switching law $\sigma(t)$ (see Figure 2). In this figure, the principle of the considered hybrid controller is described.

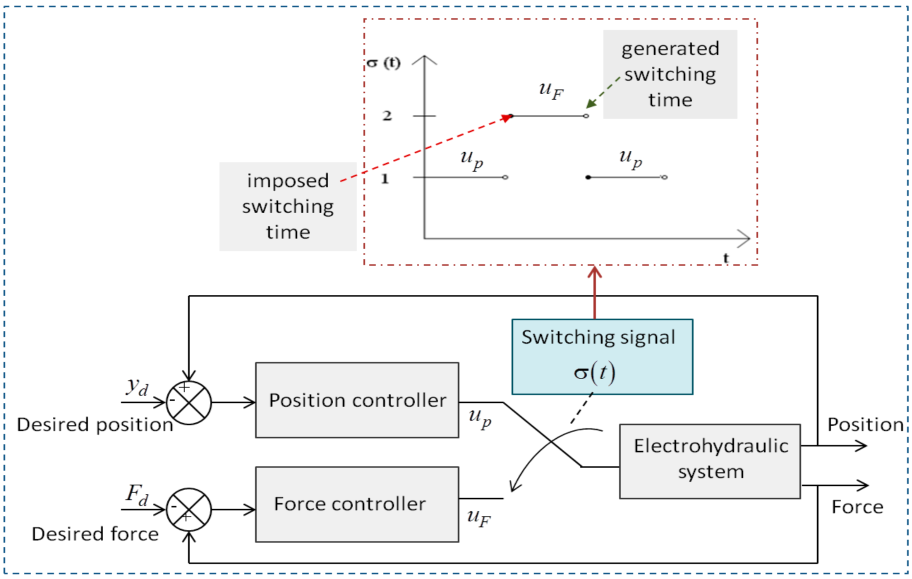

Figure 2. Principles of the hybrid controller.

Different phases must occur successively. Firstly, the position controller is started by choosing a smoothing desired position trajectory, such as a polynomial trajectory. According to our specifications, the desired trajectory for the position must have a static phase to reach some given position and remain there for a certain time. The second phase is carried out when the position reaches the static phase. Then, the closed-loop system switches from u_p to u_F over some period of time imposed by the switching signal $\sigma(t)$. In fact, to orchestrate between the two strategies' laws, the switching law must be correctly designed, especially at switching times from u_F to u_p. Indeed, these switching times will necessarily depend on the convergence time of the residual dynamics rated as T_{res}. To avoid any damages in the process, the commutation from u_F to u_p must be done after T_{res} to ensure that the residual dynamics converge to the values imposed by the position controller. The choice of this switching criterion depends on the characteristics of the load, the coefficient of the viscous friction force and the convergence time of the effort to its desired trajectory. Therefore, the design problem of the switching law consists in determining the switch occurrences that must be imposed when there is commutation from u_F to u_p, as well as the switch occurrences that must be generated when the controller switches again to the position tracking target. To illustrate the problem that may arise at the switching times when switching again to the position control, some simulation tests will be presented in the following paragraph.

3.2. Illustration of the Problem Statement

Given that the state variables are the same for both subsystems, it is important that these variables have the same values at the switching times to avoid any damage. To illustrate the switching problem that may occur, some simulation results are presented. Let us define the desired trajectory of effort F_d by a sinusoidal signal with some pulsation as follows:

$$F_d(t) = F_0 + F_{\max} \times \sin(wt), \text{ where } F_0 = Mg + ky_d(t_{sp}).$$

The desired trajectory of the position y_d is defined by the polynomial function shown in Figure 3a. $y_d(t_{sp})$ is the value of the desired position at the static phase (t_{sp}).

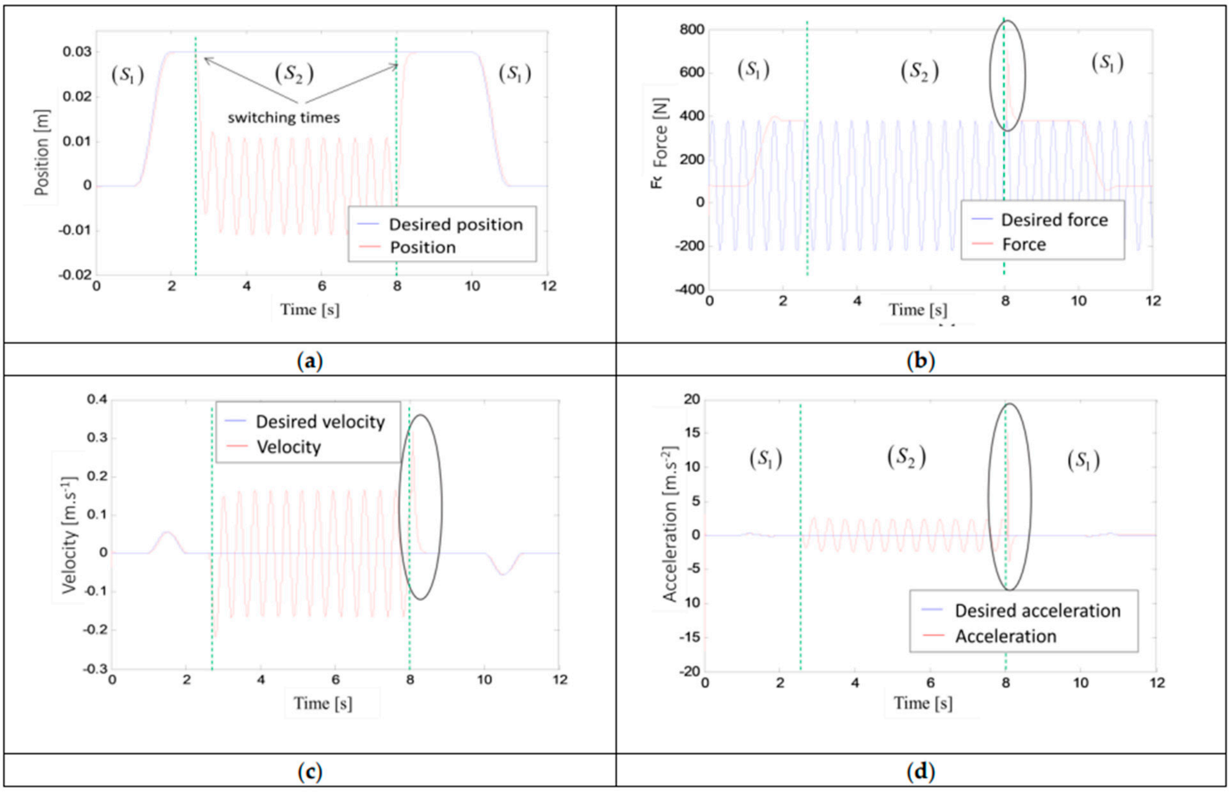

Figure 3. Illustration of the switching problem: (**a**) evolution of position (red) and its desired trajectory (blue); (**b**) evolution of force (red) and its desired trajectory (blue); (**c**) evolution of velocity (red) and its desired trajectory (blue); (**d**) evolution of acceleration (red) and its desired trajectory (blue).

In the simulation tests, the switch from (S_1) to (S_2) occurs when the position is established at the constant value, which is defined by the static phase of the desired position trajectory. In Figure 3, each switching from one subsystem to another is indicated by a green dotted line. The first switching takes place at slightly over 2 s. At more than 8 s, the second commutation one occurs.

At the end of this static phase, the switch is performed to (S_2). Figure 3b–d shows huge visible peaks on the curves of effort, velocity and acceleration. The peak recorded for effort presents maximum outracing of about 600 N. Such a value can easily damage the system. These peaks are due to the manner of switching, which occurs before the dynamic residual convergence.

4. Controller Design

Two control laws will be synthesized in this section. For the tracking control position, the backstepping technique [12] is considered. The force control law is defined using the Lyapunov method to ensure exponential convergence.

4.1. Problem Statement

Backstepping control is a design procedure developed for systems with a lower-triangular form. The key property of this technique is that it offers a constructive way of forwarding the non-reachable control to a new virtual control law. Indeed, a recursive procedure is repeated until the actual control variable is reached.

Let us start with the first subsystem (S_1), which is defined by:

$$\dot{X} = f(X) + g(X)u_p; \qquad (S_1) \tag{11}$$

The equilibrium point X^e is given by: $X^e = [y^e = 0, v^e = 0, \Delta P^e = Mg]'$, where $y^e, v^e, \Delta P^e$ are the position, the velocity and the pressure drop defined at the equilibrium point, respectively. Therefore, with a simple translation $\Delta p^e - Mg = 0$, the equilibrium point can be defined by $X^e = [0, 0, 0]'$. Note that y_d, v_d, a_d are the desired trajectories of the position, velocity and acceleration, respectively.

In order to apply the backstepping technique, different steps are considered as explained in the Figure 4. Each step is based on the definition of a virtual input, error variable, stabilizing function and the use of Lyapunov functions. The subscript i in Figure 4 represents the number of equation related to the sub-system 1.

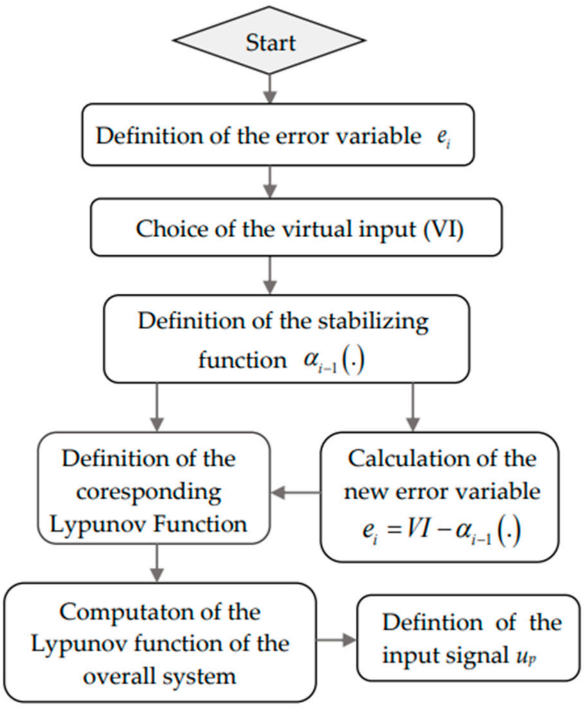

Figure 4. Basic principles of the controller position.

The expressions of $\alpha_i(.)$ and u_p are only one possible choice in order to exactly compensate the terms that come from the measurements. The details of the different calculation steps are described below.

Step 1: Let e_1 be the deviation of y from its desired value: $e_1 = y - y_d$. The derivative of the position error is computed as: $\dot{e}_1 = \dot{y} - \dot{y}_d = v - v_d$. In this step, v is viewed as the input of the first equation of (S_1). Let us define $\alpha_0(e_1, v_d)$ as a stabilizing function.

Now, the aim is to design a feedback control $v = \alpha_0(e_1, v_d)$ to stabilize the origin $e_1 = 0$. α_0, which is chosen as:

$$\alpha_0(e_1, v_d) = v_d - c_1 e_1, \tag{12}$$

where c_1 is a positive constant: $c_1[s^{-1}] > 0$. The closed-loop subsystem becomes: $\dot{e}_1 = -c_1 e_1$. For satisfying the requirement, the Lyapunov function of the first equation of (S_1) is chosen as $V_{11}(e_1) = \frac{1}{2}e_1^2$. Then, the derivative of the Lyapunov function along the solutions corresponds to:

$$\dot{V}_{11}(e_1) = e_1 \dot{e}_1 < 0 \tag{13}$$

Hence, the origin $e_1 = 0$ is globally exponentially stable.

Step 2: Since v is not an effective control of the system but rather a state variable, so a new error variable is introduced to represent the difference between this variable v considered as a virtual control and the stabilizing function $\alpha_0(.)$, as defined in (12). Consider a new error variable e_2 defined as the difference between the virtual input v and the associated stabilizing function as following:

$$e_2 = v - \alpha_0(e_1, v_d) = v - v_d + c_1 e_1 = \dot{e}_1 + c_1 e_1 \tag{14}$$

According to the variables e_1 and e_2, the (y, v) subsystem is transformed to the following form:

$$\begin{cases} \dot{e}_1 = -c_1 e_1 + e_2 \\ \dot{e}_2 = \ddot{e}_1 + c_1 \dot{e}_1 = a - a_d + c_1(e_2 - c_1 e_1) \end{cases} \tag{15}$$

Consider now Δp as the new virtual input of the system error described above. In this case, the Lyapunov function V_{12} is constructed by augmenting V_{11} with a quadratic term in the error variable e_2 :

$$V_{12}(e_1, e_2) = V_{11}(e_1) + \frac{1}{2}(v - \alpha_0(e_1, v_d))^2 = V_{11}(e_1) + \frac{1}{2}e_2^2 \tag{16}$$

Then, the derivative of e_2 is given by:

$$\dot{e}_2 = \frac{S}{M}\left[\frac{1}{S}\left[e_2(-b + c_1 M) + e_1\left(bc_1 - kM - c_1^2 M\right) - (bv_d + ky_d + Mg + Ma_d)\right] + \Delta P \quad \right] \tag{17}$$

Let us now define $\alpha_1(e_1, e_2, y_d, v_d, a_d)$ as a new stabilizing function. After that, feedback control is chosen as $\Delta P = \alpha_1(.)$:

$$\alpha_1(e_1, e_2, y_d, v_d, a_d) = \frac{1}{S}[-e_2(-b + c_1 M) - e_1\left(bc_1 - kM - c_1^2 M\right) + (bv_d + ky_d + Mg + Ma_d) - c_2 e_2] \tag{18}$$

Subsisting the previous equation in the derivative of V_{12} :

$$\dot{V}_{12}(e_1, e_2) = \dot{V}_{11}(e_1) - c_2 e_2^2 = -c_1 e_1^2 - c_2 e_2^2 < 0, \tag{19}$$

where c_2 is a positive constant: $c_2[s^{-1}] > 0$. From (14), we deduce that the origin $e_1 = e_2 = 0$ is stable.

Step 3: Let us define a third variable error e_3 as: $e_3 = \Delta P - \alpha_1(e_1, e_2, y_d, v_d, a_d)$. From the defined variables errors, (S_1) can be re-written as follows:

$$\begin{cases} \dot{e}_1 = -c_1 e_1 + e_2, \\ \dot{e}_2 = \frac{S}{M} e_3 - c_2 e_2, \\ \dot{e}_3 = \Delta\dot{P} - \dot{\alpha}_1(e_1, e_2, y_d, v_d, a_d) \end{cases} \tag{20}$$

Then, the Lyapunov function of the overall system can be expressed by adding V_{12} with the quadratic term in e_3:

$$V_1(e_1, e_2, e_3) = \frac{1}{2}c_1 e_1^2 + \frac{1}{2}c_2 e_2^2 + \frac{1}{2}c_3 e_3^2 \tag{21}$$

where c_3 is a positive gain: $c_3[s^{-1}] > 0$. Therefore, to ensure that $V_1 < 0$, the control law u_p is chosen as:

$$u_p = \frac{1}{\beta\left[\frac{r\psi_1(p_1, sign(u))}{V_1(y)} + \frac{r\psi_2(p_2, sign(u))}{V_2(y)}\right]} \times \left[\beta S\left(\frac{1}{V_1(y)} + \frac{1}{V_2(y)}\right)v + \dot{\alpha}_1(e_1, e_2, y_d, v_d, a_d) - c_3 e_3 \right] \tag{22}$$

It is clear that the singularity of Equation (22) occurs when $\psi_1(.) = \psi_2(.) = 0$, which is the case when the pressures in the two chambers are equal, respectively, to the supply and the exhaust pressure. Or, according to the defined physical domain D_φ, this problem is avoided. Hence, the origin of (S_1) is globally asymptotically stable.

4.2. Force Controller

The second system has the same vectors fields as (S_1), but the control law is replaced by u_F. Indeed, in the current case, the force output is controlled, where the subsystem (S_2) is defined by:

$$\dot{X} = f(X) + g(X)u_F; \qquad (S_2) \tag{23}$$

Let the Lyapunov function be defined as:

$$V_2 = \frac{1}{2}(F(t) - F_d(t))^2 = \frac{1}{2}e_F^2(t) \tag{24}$$

where F is the force of the hydraulic fluid on the piston and F_d is its desired trajectory, which is assumed to be a C^∞ differentiable function.

The equilibrium point $X^e = [0, 0, 0]'$, the following condition $V_2(0) = 0$ is easily checked. Differentiating (24) along the system trajectories, we obtain:

$$\dot{V}_2 = (F(t) - F_d(t))\left(\dot{F}(t) - \dot{F}_d(t)\right) \tag{25}$$

The expression of the hydraulic force is given by:

$$\dot{F} = S\Delta\dot{P} = -\beta S^2\left[\frac{1}{V_1(y)} + \frac{1}{V_2(y)}\right]v + \beta\left[\frac{r\psi_1(p_1, sign(u))}{V_1(y)} + \frac{r\psi_2(p_2, sign(u))}{V_2(y)}\right]u_F \tag{26}$$

$$u_F = \frac{1}{\beta\left[\frac{r\psi_1(p_1, sign(u))}{V_1(y)} + \frac{r\psi_2(p_2, sign(u))}{V_2(y)}\right]} \times \left[S^2\beta\left(\frac{1}{V_1(y)} + \frac{1}{V_2(y)}\right)v + \varphi(t)\right] \tag{27}$$

where $\psi_1(.)$ and $\psi_2(.)$ are the same nonzero quantities defined in (6). By replacing the expression of u_F into (26), we obtain:

$$\dot{F} = \varphi(t) \tag{28}$$

To have an exponential convergence of e_F, the function $\varphi(t)$ can be selected as follows:

$$\varphi(t) = \dot{F}_d - K_f(F - F_d) \tag{29}$$

where K_f is a positive gain. Replacing (29) in (28), we obtain the following equation:

$$\dot{F} = \dot{F}_d - K_f(F - F_d) \Rightarrow \dot{e}_F = -K_f e_F(t) \tag{30}$$

The solution of the previous equation guarantees the exponential force stabilization:

$$e_F(t) = e^{-K_f t} e_F(0) \tag{31}$$

The convergence time is adjusted by the gain K_f. Now, substituting the previous Equation into (30) gives:

$$\dot{V}_2 = -K_f(F - F_d)^2 = -2K_f V_2 \Rightarrow \dot{V}_F \leq 0 \tag{32}$$

Therefore $\dot{V}_2$ is a negative definite function. Note that $\dot{V}_2$ is a differentiable function, where $\ddot{V}_2$ exists and is bounded. Then, with Barbalat's lemma, the asymptotic stability can be deduced. However, the overall stability of (S_2) depends on the stability of the uncontrolled dynamics. These dynamics are represented by the following linear state space:

$$\dot{X}_{res} = A.X_{res}(t) + BE_{res}(t) \tag{33}$$

where: $X_{res} = \begin{bmatrix} y & v \end{bmatrix}^T$, $E_{res} = (S\Delta P - Mg)$ are the inputs of the linear system and the matrix A, B are defined by:

$$A = \begin{bmatrix} 0 & 1 \\ -k/M & -b/M \end{bmatrix}; B = \begin{bmatrix} 0 \\ \frac{1}{M} \end{bmatrix}$$

The characteristic polynomial of (33) is given by:

$$\pi(s) = s^2 + \frac{b}{M}s + \frac{k}{M} = 0 \tag{34}$$

where s is a complex number frequency parameter. Equation (34) represents a Hurwitz characteristic polynomial. From the bounded-input bounded-output (BIBO) stability, the residual dynamics can also be stable. Indeed, the input signal E_{res} of the linear system (33) is always bounded, and, with the physical domain D_φ, all state variables are bounded, which easily justifies the stability of these dynamics.

5. Proposed Solution

To address the problem of our work, a reference trajectory generator of the effort is proposed, and it will be updated during the system operation. This update requires adding a dead zone Δt_{ZM} in the effort trajectory to enable the necessary time for the residual dynamics T_{res} to converge properly to the values imposed by (S_1). To calculate T_{res}, it is necessary to have some information about the system state variables. Figure 5 describes the proposed solution. As shown in this figure, the values $y(t_{ZM}), v(t_{ZM})$, which are, respectively, the position and the velocity at the beginning of the force static phase, must be measured. Furthermore, the error values of the position, velocity and force must be imposed in order to achieve a given accuracy.

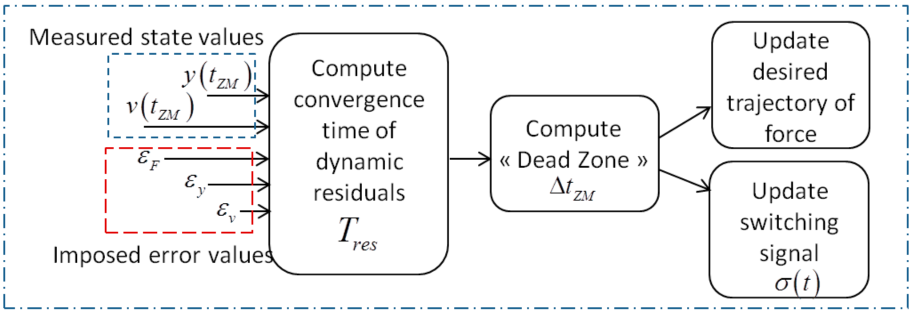

Figure 5. Principle of the proposed solution: case $(S_2)\rightarrow(S_1)$.

Therefore, the width of this dead zone is then used to update the switching signal. Therefore, this last one can be defined by:

- the imposed switching times when (S_1) commutes to (S_2)
- the generated switching times when (S_2) commutes to (S_1)

To compute T_{res} and Δt_{ZM}, our proposal is developed below.

The solution of (33) is defined by the following expression:

$$X_{res}(t) = e^{A(t-t_{ZM})}.X_{res}(t_{ZM}) + \int_{t_{ZM}}^{t} e^{A(t-\tau)}B.E_{res}(t)d\tau \tag{35}$$

where t_{ZM} is the time at which $F_d = F_0$, with $F_0 = ky_d(t_{sp}) + Mg$ the effort given by the static phase during the position controller.

The main idea of the solution is to find an approximation of T_{res} under certain considerations that will be presented. Therefore, consider that $|e_F| = |F - F_d| < \varepsilon_{F_{res}}$, where $\varepsilon_{F_{res}}$ is an imposed value. The velocity of convergence of the residual dynamics depends on the real part of the roots of the characteristic polynomial. Then, the convergence time of the residual dynamics for each kind of the characteristic equation roots will be estimated. For this, the following inequality must be solved:

$$\begin{array}{l} Find\ T_{res}\ with\ T_{res}\ > t_{ZM} \\ \text{where} |X(t)| = |X_d(t)|, \quad \forall t \geq T_{res} \end{array}$$

$X_d(t)$ represents the vector of residual dynamic values when (S_1) is active. Then, we can replace this last inequality by:

$$Find\ T_{res}\ /\ T_{res}\ > t_0\ /\ |\varepsilon_X(t)| \leq \varepsilon_{Xd}$$

With: $\varepsilon_X = \begin{bmatrix} \varepsilon_{X(1)} \\ \varepsilon_{X(2)} \end{bmatrix} = \begin{bmatrix} X_{(1)} = y \\ X_{(2)} = v \end{bmatrix} - \begin{bmatrix} X_{d1} \\ X_{d2} \end{bmatrix}$, where X_{d1} and X_{d2} are the imposed values, respectively, for the position and the velocity, which are defined by the static phase relative to the servo positioning. $\varepsilon_{X(1)}$ and $\varepsilon_{X(2)}$ are the pre-defined error values, and it is necessary to set them as low as possible.

Knowing that the matrix A has a companion form, the following variable change from the state X_{res} to ξ can be defined as:

$$\begin{array}{c} X_{res} = P\xi \Rightarrow \dot{\xi}(t) = \left(P^{-1}AP\right)\xi + P^{-1}BE_{res} \\ \Rightarrow \dot{\xi}(t) = Q\xi + B'E_{res} \end{array} \tag{36}$$

where P is the transformation matrix and Q is a matrix of the diagonal or Jordan form. Then, the exponential of the matrix A is given as follows:

$$A = PQP^{-1} \Rightarrow e^{At} = Pe^{Qt}P^{-1} \tag{37}$$

For each case, the convergence time of the residual dynamics T_{res} is determined and is described above.

Let us define $X_{(01)} = X_{(1)}(t_{ZM}) = y(t_{ZM}), \quad X_{(02)} = X_{(2)}(t_{ZM}) = v(t_{ZM})$, where $X_{(0)} = \left[X_{(01)}, X_{(02)}\right]^T$ and λ_1, λ_2 are the roots of the characteristic polynomial of (33). Therefore, depending on the sign of the discriminant of this polynomial, three cases can occur.

Case 1: For $\Delta < 0$,($\lambda_{1,2}$ conjugated complex roots)

For the first case, the form of the matrix P can be written as:

$$P = \begin{bmatrix} 1 & 1 \\ \lambda_1 & \lambda_2 \end{bmatrix} \Rightarrow P^{-1} = \frac{1}{(\lambda_2 - \lambda_1)} \begin{bmatrix} \lambda_2 & -1 \\ -\lambda_1 & 1 \end{bmatrix}.$$

Assuming that $\Gamma = \frac{1}{(\lambda_2 - \lambda_1)}$, then we have:

$$|X| = \begin{bmatrix} X_{(1)} \\ X_{(2)} \end{bmatrix} \leq \left|e^{A\Delta t}\right| \times \begin{bmatrix} X_{(01)} \\ X_{(02)} \end{bmatrix} \tag{38}$$

Therefore,

$$|X| \leq \left|e^{A\Delta t} X_0\right| + \int_{t_{ZM}}^{t_{res}} \left|e^{A(t_{res}-\theta)} B\right| |\varepsilon_{F_{res}}| d\theta \tag{39}$$

From these two inequalities (38) and (39), we can extract two equations thus:

$$\begin{aligned} \left|X_{(1)}\right| \leq & \left[\left|\frac{X_{(01)}}{\Gamma}\left(\lambda_1 e^{\lambda_1 \Delta t_1} - \lambda_1 e^{\lambda_2 \Delta t_1}\right)\right| + \left|\frac{X_{(02)}}{\Gamma}\left(\lambda_2 e^{\lambda_2 \Delta t_1} - \lambda_1 e^{\lambda_2 \Delta t_1}\right)\right|\right] \\ & + \int_{t_{ZM}}^{t_{res}} \left|\frac{1}{\Gamma M}\left(e^{\lambda_2 (t_{res} - \Delta t_1)} + e^{\lambda_1 (t_{res} - \Delta t_1)}\right)\right| |\varepsilon_{F_{res}}| \leq \varepsilon_{X_{(1)}} \end{aligned}$$

$$\begin{aligned} \left|X_{(2)}\right| \leq & \left[\left|X_{(01)}\left(\frac{\lambda_1 \lambda_2}{\Gamma} e^{\lambda_1 \Delta t_2} - \lambda_2 e^{\lambda_2 \Delta t_2}\right)\right| + \left|X_{(02)}\left(\frac{\lambda_2}{\Gamma} e^{\lambda_2 \Delta t_2} - \frac{\lambda_1}{\Gamma} e^{\lambda_1 \Delta t_2}\right)\right|\right] \\ & + \int_{t_{ZM}}^{t_{res}} \left| -\frac{\lambda_1}{\Gamma M} e^{\lambda_1 (t_{res} - \Delta t_2)} + \frac{\lambda_2}{\Gamma M} e^{\lambda_2 (t_{res} - \Delta t_2)}\right| |\varepsilon_{F_{res}}| \leq \varepsilon_{X_{(2)}} \end{aligned}$$

From the first inequality of the above system, the convergence time approximation of y is given by:

$$t_{res1} \geq t_{ZM} - \frac{1}{|d|} \log\left(\left|\frac{\varepsilon_{X_{(1)}} - 2\frac{\varepsilon_{F_{res}}}{M|d||\Gamma|}}{\phi_1}\right|\right) \tag{40}$$

where:

$$\phi_1 = 2\frac{\varepsilon_{F_{res}}}{M|d||\Gamma|} - 2\left|X_{(01)}\right| \frac{\lambda}{|\Gamma|} - 2\frac{\left|X_{(02)}\right|}{|\Gamma|}$$

And $d = \Re e(\lambda_1) = \Re e(\lambda_2), \quad |\lambda| = |\lambda_{1,2}| = \sqrt{(\Re e(\lambda_{1,2}))^2 + (\Im m(\lambda_{1,2}))^2}$. From the second inequality, the convergence time of v is computed by:

$$t_{res2} \geq t_{ZM} - \frac{1}{|d|} \log\left(\left|\frac{\varepsilon_{X_{(2)}} - 2\frac{\varepsilon_{F_{res}}|\lambda|}{M|d||\Gamma|}}{\phi_2}\right|\right) \tag{41}$$

where

$$\phi_2 = 2\frac{|\lambda|\varepsilon_{F_{res}}}{M|d||\Gamma|} - 2\frac{\lambda^2\left|X_{(01)}\right|}{|\Gamma|} - 2\frac{\left|\lambda X_{(02)}\right|}{|\Gamma|}.$$

Case 2: For $\Delta < 0$,($\lambda_{1,2}$ Real roots)

For the real roots, the convergence times t_{res1},t_{res2} of y and v, respectively, can be deduced. We start with the following expression for y:

$$t_{res1} \geq t_{ZM} - \frac{1}{|\lambda_2|} \log\left(\left|\frac{\phi_3}{\phi_4}\right|\right) \tag{42}$$

where:

$$\phi_3 = \frac{1}{|\Gamma|}\left(|\lambda_1| - 1 + \frac{1}{M|\lambda_2|}\right); \quad \phi_4 = \varepsilon_{X_{(1)}} + \frac{1}{M|\Gamma|}\left(\frac{1}{|\lambda_1|} + \frac{1}{|\lambda_2|}\right)$$

For v,

$$t_{res2} \geq t_{ZM} - \frac{1}{|\lambda_2|} \log\left(\left|\frac{\phi_5}{\phi_6}\right|\right) \tag{43}$$

where:

$$\phi_5 = \varepsilon_{X_{(2)}} - \frac{2}{M|\Gamma|}; \quad \phi_6 = -\frac{|\lambda_1\lambda_2|}{|\Gamma|} + \frac{1}{M|\Gamma|}(1 + |\lambda_2|)$$

Case 3: For $\Delta = 0$,($\lambda_1 = \lambda_2 = \lambda$ is the double root)

In this particular case, we have $\frac{k}{M} = \frac{b^2}{4M^2}$, and the transformation matrix P is written as follows:

$$P = \begin{bmatrix} 1 & 0 \\ \lambda & 1 \end{bmatrix} \Rightarrow P^{-1} = \begin{bmatrix} 1 & 0 \\ -\lambda & 1 \end{bmatrix}; \quad Q = \begin{bmatrix} \lambda & 1 \\ 0 & \lambda \end{bmatrix}$$

The convergence times t_{res1}, t_{res2} are determined by Equations (44) and (45):

$$t_{res_1} \geq t_{ZM} - \frac{\phi_7}{\phi_8}|\lambda| \tag{44}$$

where

$$\phi_7 = |\lambda|\phi_9 + \phi_8 LambertW\left[-\frac{|\lambda|\phi_{10}e^{-\frac{|\lambda|\phi_9}{\phi_8}}}{\phi_8}\right];$$

$$\phi_9 = \left|X_{(01)}\right| - \frac{1}{M|\lambda|^2}; \phi_8 = \left|X_{(02)}\right| - |\lambda|\left|X_{(01)}\right| - \frac{1}{M|\lambda|} \text{ and } \phi_{10} = \varepsilon_{X_{(1)}} - \frac{1}{M|\lambda|^2}.$$

$$t_{res_1} \geq t_{ZM} - \frac{\phi_7}{\phi_8}|\lambda| \tag{45}$$

where

$$\phi_{11} = \lambda\left|X_{(02)}\right| + \phi_{12} LambertW\left[-\frac{|\lambda|\varepsilon_{X_2}\phi_{13}}{\phi_{12}}\right]; \phi_{12} = \left|X_{(02)}\right|\left(\lambda^2 - 1\right) + \varepsilon_{F_{res}};$$
$$\phi_{13} = e^{-\frac{|\lambda X_{(02)}|}{\phi_{12}}}.$$

Finally, for each study case, the convergence time of the residual dynamics corresponds to the slowest one. This allows us to write:

$$T_{res} = Max(t_{res1}, t_{res2}). \tag{46}$$

where t_{res1} and t_{res2} are the approximations of the convergence times of the position and the velocity, respectively, which are generally computed as:

$$t_{res1} \geq t_{ZM} - \chi_i\left(y(t_{ZM}), v(t_{ZM}), \varepsilon_{F_{res}}, \varepsilon_y, \varepsilon_v, \lambda_1, \lambda_2\right); \quad where \quad i \in \{1,2\} \tag{47}$$

χ_i is a function that depends on such parameters as the errors of variables $\varepsilon_{F_{res}}, \varepsilon_y, \varepsilon_v$ and characteristics of the load. λ_1, λ_2 are the roots of the characteristic polynomial of (35) and $y(t_{ZM}), v(t_{ZM})$ are, respectively, the position and the velocity corresponding to the measured state values at the beginning of the dead zone.

6. Validation of the Proposed Solution

We performed some simulation tests to illustrate the controller/switching signal design shown above. The control system model and the control law were implemented on the Simulink software. The selected sampling frequency was equal to 1 kHz. For these simulations, the stiffness of the load was equal to 1000 N/m. The proposed solution requires knowledge of tracking errors that remain arbitrary depending on the specification. For our case, we had $\varepsilon_y = 10^{-6}; \varepsilon_v = 10^{-6}$ and $\varepsilon_{F_{res}} = 10^{-3}$. The simulations were performed with a reference position trajectory which is defined by polynomial function that has some static phases (see Figure 6). In addition, a sinusoidal desired effort trajectory was used (Figure 7).

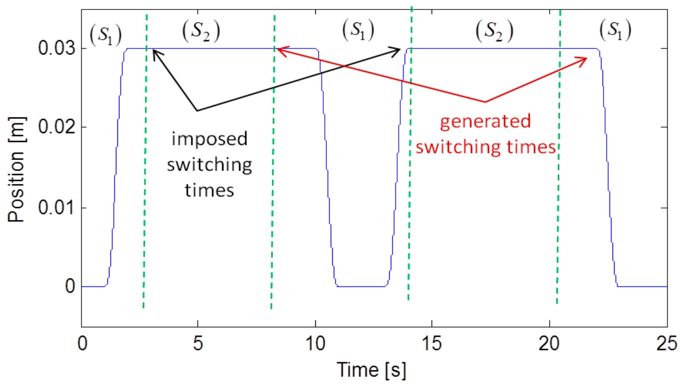

Figure 6. Evolution of the desired position.

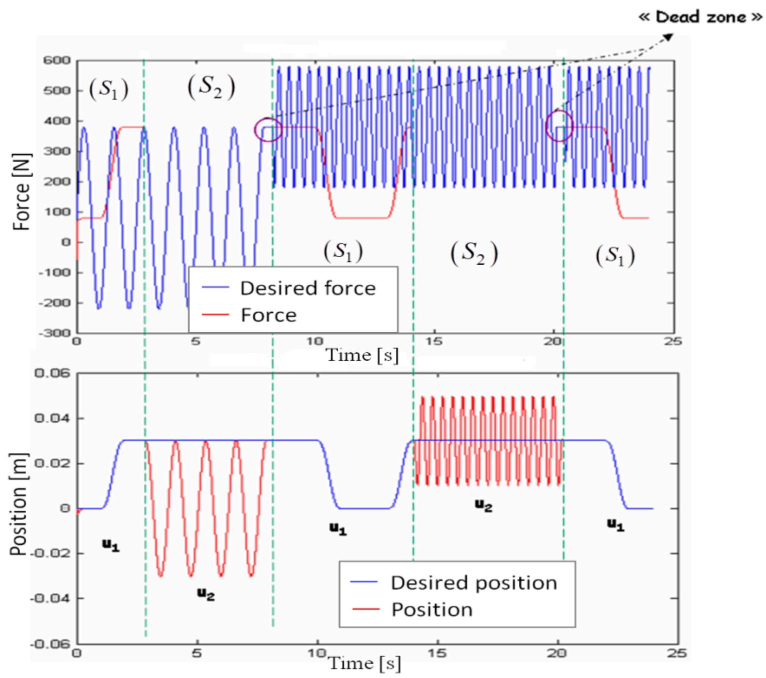

Figure 7. Evolution of the effort (**upper**) and the position (**below**) with their desired trajectories.

7. Discussion

We began the simulation tests by activating the subsystem (S_1). When the position reached the static phase imposed by its desired trajectory, the subsystem (S_2) was activated to control an applied force on the load. We observe from Figures 7 and 8 that, when the proposed method was applied, there were no adverse effects on the system status. Further, the simulation test was performed even with a variable frequency of the desired effort trajectory to solicit different dynamics applied to the load.

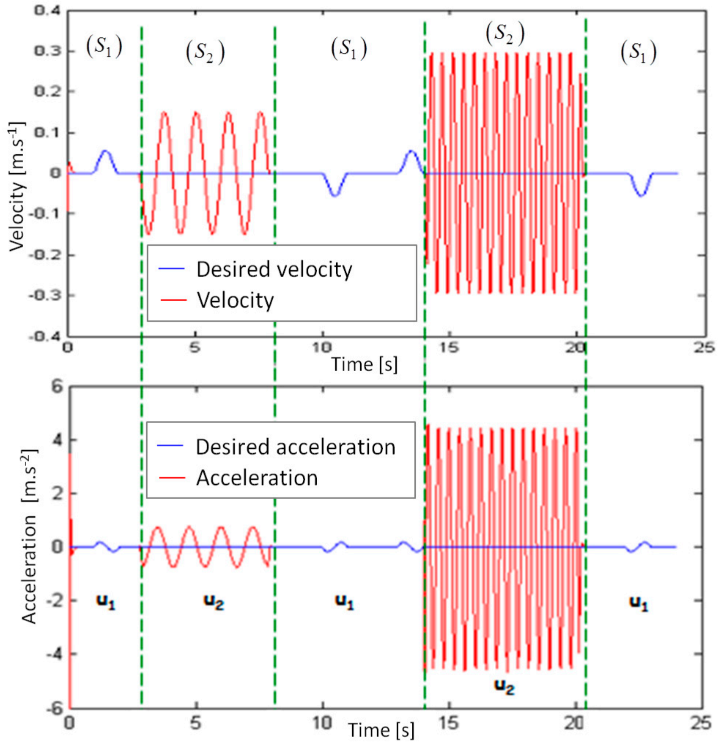

Figure 8. Evolution of the velocity (**upper**) and the acceleration (**below**) with their desired trajectories.

As shown in Figure 7, there are more than two switches for the position controller, so it is necessary in this case to impose two dead zones ($T_{ZM(1)}$ and $T_{ZM(2)}$) in the desired trajectory of the effort. Therefore, a desired generator trajectory of the effort was updated. Then, the computation of the width of the dead zones was carried out using Equation (47).

When the subsystem (S_2) was activated, the effort was under control but not the displacement. At this stage, we noticed that the effort was very close to the desired pre-calculated trajectory of the effort (see Figure 7 upper). On the other hand, the displacement did not follow its desired trajectory, but, under the effect of a causal relationship between these two physical variables, the displacement will be of the same form as the effort trajectory.

Figure 8 shows some modifications to the trajectories of the velocity and the acceleration, as well as their desired trajectories. From this figure, good trajectory tracking is shown for the synthesized hybrid position/effort controller. We can conclude that the simulation test allowed direct validation of the hybrid position/force controller and the proposed solution in order to impose switching times that ensured no adverse effects in terms of tracking the trajectories.

The results obtained show the efficiency of automation of time-dependent switching signals. This is generated via the definition of a force trajectory generator that is updated instantaneously according to system conditions. This update prevents harmful problems that may be caused by the residual dynamics. Indeed, any undesirable effect on speed and acceleration is avoided. In addition, it should be noted that the controller has a good follow-up of the desired trajectories, whether for the position or the effort.

By referring to the work carried out in Ref. [32], we have proposed another hybrid position/force control approach. This approach in Ref. [32] was based on a linearized control model in which the structure of the control law remained the same and only the parameterization changed. The switching signal used was based on a hysteresis function. Admittedly, the tracking quality was good, but the peaks of the effort during transitions were recorded. On the other hand, our current approach consists in automatically generating the force trajectory in order to avoid these peaks and, thus, all damage to the system.

The trajectory generator is defined by a mathematical calculation taking into account the residual dynamics.

8. Conclusions

In this paper, a hybrid controller for an electrohydraulic servo-actuator with residual dynamics has been studied to verify its BIBO stability. To achieve this aim, a method for automatically generating the desired effort trajectory has been outlined in order to design a real-time switching signal. The proposed solution makes it possible to switch between the two control laws without damage and to avoid all the peaks in the states. Many points of view could be explored for future studies. First, the parametric uncertainties in the model should be considered since the load characteristics may well be unknown. Another one is to carry out some experimental results on the system.

Author Contributions: Conceptualization, L.S. and I.C.; methodology, L.S. and I.C.; software, L.S., I.C. and M.S.; validation, L.S., I.C. and M.S.; formal analysis, L.S., I.C. and M.S.; investigation, L.S., I.C. and M.S.; resources, L.S., I.C. and M.S.; data curation, L.S., I.C. and M.S.; writing original draft preparation, L.S., I.C. and M.S.; writing—review and editing, L.S., I.C. and M.S. All authors have read and agreed to the published version of the manuscript.

Funding: This research received no external funding.

Data Availability Statement: Data sharing not applicable.

Conflicts of Interest: The authors declare no conflict of interest.

Appendix A

Table A1. Hydraulic actuator characteristics.

Piston diameter	50 mm
Rod diameter	30 mm
Total moving load	5.9 kg
Length max	166 mm
Supply pressure p_P	210 bar
Maximum static force	19,858 $N \quad for\ p_P = 210$ bar
Maximum dynamic force	3238 $N \quad for\ p_P = 210$bar

References

1. Merrit, H.E. *Hydraulic Control Systems*; John Wiley and Sons: Hoboken, NJ, USA, 1976.
2. Andersen, T.O.; Hansen, M.R.; Pedersen, H.C.; Conrad, F. Comparison of linear controllers for a hydraulic servo system. In Proceedings of the 6th JFPS International Symposium on Fluid Power, Tsukuba, Japan, 7–10 November 2005; pp. 7–10.
3. Aly, A.A. PID Parameters Optimization Using Genetic Algorithm Technique for Electrohydraulic Servo Control System. *Intell. Control Autom.* **2011**, *2*, 69–76. [CrossRef]
4. Brunton, S.; Kutz, J. Linear Control Theory. In *Dynamical Systems, and Control*; Cambridge University Press: Cambridge, UK, 2019; pp. 276–320.
5. Sidhom, L.I.; Chihi, I.; Sahraoui, S.; Abdelkrim, A. PI-intelligent controller for electro-hydraulic system. In Proceedings of the IEEE International Conference on Control Engineering & Information Technology (CEIT), Hammamet, Tunisia, 16–18 December 2016.
6. Re, L.D.; Isidori, A. Performance enhancement of nonlinear drives by feedback linearization of linear-bilinear cascade models. *IEEE Trans. Control Syst. Technol.* **1995**, *3*, 299–308.
7. Ferestade, I.; Molatefi, H.; Moaveni, B. Parallel Structure of Feedback Linearization and Sliding Mode Controllers to Track the Desired Velocity Profile in High-Speed Trains. In *Mathematical Problems in Engineering*; Hindawi: London, UK, 2021; Volume 2021, p. 7637023.
8. Plummer, A.R.; Vaughan, N.D. Robust adaptive control for hydraulic servo systems. *ASME J. Dyn. Syst. Meas. Control* **1996**, *118*, 237–244. [CrossRef]
9. Yao, J.; Deng, W.; Jiao, Z. Adaptive Control of Hydraulic Actuators with LuGre Model-Based Friction Compensation. *IEEE Trans. Ind. Electron.* **2015**, *62*, 6469–6477. [CrossRef]
10. Mahmoud, I.; Chihi, I.; Abdelkrim, A. Adaptive Control Design for Human Handwriting Process Based on Electromyography Signals. In *Complexity*; Wiley Hindawi: Hoboken, NJ, USA, 2020; Volume 2020, p. 5142870.

11. Sidhom, L.; Smaoui, M.; Brun, X.; Bideaux, E. Robust Estimator Design for Control of Electropneumatic System. *IETE J. Res.* **2018**, *64*, 689–701. [CrossRef]
12. Sidhom, L.; Brun, X.; Smaoui, M.; Bideaux, E.; Thomasset, D. Dynamic Gains Differentiator for Hydraulic System Control. *J. Dyn. Syst. Meas. Control* **2015**, *137*, 041017. [CrossRef]
13. Yao, J.; Yang, G.; Jiao, Z. High dynamic feedback linearization control of hydraulic actuators with backstepping. *J. Syst. Control Eng.* **2015**, *229*, 728–737. [CrossRef]
14. Guan, C.; Pan, S. Adaptive sliding mode control of electro-hydraulic system with nonlinear unknown parameters. *Control Eng. Pract.* **2008**, *16*, 1275–1284. [CrossRef]
15. Gupta, P.; Huang, S.; Huang, J.; Cai, Z.; Cui, H. Adaptive Backstepping Sliding Mode Control for Quadrotor UAV. In *Scientific Programming*; Hindawi: London, UK, 2021; Volume 2021, p. 3997648.
16. Wang, Z.; Zhu, S.; Chen, Q.; Zhang, X.; Song, Y. Sliding mode control of electro-hydraulic servo system for lower-limb exoskeleton based on RBF neural network. In Proceedings of the IEEE 10th Conference on Industrial Electronics and Applications, Auckland, New Zealand, 15–17 June 2015; pp. 15–17.
17. Zhang, C. Sliding mode observer and controller design for a hydraulic motion control system Batur. In Proceedings of the American Control Conference, Denver, CO, USA, 3–6 February 2003; 2003; 2, pp. 1721–1726.
18. Ferestade, I.; Ahmadian, M.; Molatefi, H.; Moaveni, B.; Bokaeian, V. Integrated sliding mode and direct torque controls for improving transient traction in high-speed trains. *J. Vib. Control* **2021**, *27*, 629–650. [CrossRef]
19. Wang, R.; Gao, L.; Bai, C.; Sun, H. U-Model-Based sliding mode controller design for quadrotor UAV control systems. *Math. Probl. Eng.* **2020**, *2020*, 4343214. [CrossRef]
20. Karpenko, M.; Sepehri, N. On quantitative feedback design for robust position control of hydraulic actuators. *Control Eng. Pract.* **2010**, *18*, 289–299. [CrossRef]
21. Rafiee, A.; Batmani, Y.; Ahmadi, F.; Bevrani, H. Robust Load-Frequency Control in Islanded Microgrids: Virtual Synchronous Generator Concept and Quantitative Feedback Theory. *IEEE Trans. Power Syst.* **2021**, *36*, 5408–5416. [CrossRef]
22. Nguyen, Q.H.; Ha, Q.P.; Rye, D.C.; Durrant-Whyte, H.F. Force/Position tracking for electrohydraulic systems of a robotic excavator. In Proceedings of the 39th IEEE Conference on Decision and Control (Cat. No. 00CH37187), Sydney, Autralia, 12–15 December 2000.
23. Gao, C.; Cong, D.; Liu, X.; Yang, Z.; Tao, H. Hybrid position/force control of 6-dof hydraulic parallel manipulator using force and vision. *Ind. Robot. Int. J.* **2016**, *43*, 274–283. [CrossRef]
24. Kumar, N.; Panwar, V.; Sukavanam, N.; Shama, S.P.; Borm, J.-H. Neural Network Based Hybrid Force/Position Control for Robot Manipulators. *Int. J. Precis. Eng. Manuf.* **2011**, *12*, 419–426. [CrossRef]
25. Cheah, C.C.; Kawamura, S.; Arimoto, S. Brief Stability of hybrid position and force control for robotic manipulator with kinematics and dynamics uncertainties. *Automatica* **2003**, *39*, 847–855. [CrossRef]
26. Linjama, M.; Huova, M.; Huhtala, K. Model-based force and position tracking control of an asymmetric cylinder with a digital hydraulic valve. *Int. J. Fluid Power* **2016**, *17*, 163–172. [CrossRef]
27. Dindorf, R.; Wos, P. Force and position control of the integrated electro-hydraulic servo-drive. In Proceedings of the 20th International Carpathian Control Conference (ICCC), Krakow-Wieliczka, Poland, 26–29 May 2019.
28. Pratumsuwan, P.; Junchangpood, A. Force and Position Control in the Electro-Hydraulic System by using a MIMO Fuzzy Controller. In Proceedings of the IEEE 8th Conference on Industrial Electronics and Applications (ICIEA), Melbourne, Australia, 19–21 June 2013.
29. Xie, S.; Ren, J. A Hybrid Position/Force Controller for Joint Robots. In Proceedings of the IEEE International Conference on Robotics and Automation (ICRA), Xi'an, China, 30 May–5 June 2021.
30. Mattila, J.; Koivumäki, J.; Caldwell, D.G.; Semini, C. A Survey on Control of Hydraulic Robotic Manipulators with Projection to Future Trends. *IEEE/ASME Trans. Mechatron. J.* **2017**, *22*, 669–680. [CrossRef]
31. Brun, X.; Thomasset, D.; Scavarda, S. Hybrid Control for switching between position and force tracking. In Proceedings of the 4th International Symposium on Fluid Power Transmission and Control, Wuhan, China, 8–10 April 2003; pp. 44–49.
32. Pasolli, P.; Ruderman, M. Hybrid Position/Force Control for Hydraulic Actuators. In Proceedings of the 28th IEEE Mediterranean Conference on Control and Automation (MED), Saint-Raphael, France, 15–18 September 2020.
33. Ameur, O.; Massioni, P.; Scorletti, G.; Brun, X.; Smaoui, M. Lyapunov stability analysis of switching controllers in presence of sliding modes and parametric uncertainties with application to pneumatic systems. *IEEE Trans. Control Syst. Technol.* **2016**, *24*, 1953–1964. [CrossRef]
34. Liberzon, D.; Morse, A.S. Basic problems in stability and design of switched systems. *IEEE Control Syst. Mag.* **1999**, *19*, 59–70.
35. Branicky, M.S. Stability of switched and hybrid systems. In Proceedings of the 33rd IEEE Conference on Decision and Control, Lake Bwna Vita, FL, USA, 14–16 December 1994.
36. Branicky, M.S. Multiple lyapunov functions and other analysis tools for switched and hybrid systems. *IEEE Trans. Autom. Control* **1998**, *43*, 475–482. [CrossRef]

37. Margaliota, M.; Liberzon, D. Lie-algebraic stability conditions for nonlinear switched systems and differential inclusions. *Syst. Control Lett.* **2006**, *55*, 8–16. [CrossRef]
38. Zhai, G.; Matsune, I.; Imae, J.; Kobayashi, T. A note on multiple Lyapunov functions and stability condition for switched and hybrid systems. In Proceedings of the 16th IEEE International Conference on Control Applications Part of IEEE Multi-Conference on Systems and Control, Singapore, 1–3 October 2007.